

Cite this: DOI: 10.1039/c1ee02092g

www.rsc.org/ees

PAPER

## Solution-based fabrication of vanadium dioxide on F:SnO<sub>2</sub> substrates with largely enhanced thermochromism and low-emissivity for energy-saving applications

Zongtao Zhang,<sup>ab</sup> Yanfeng Gao,<sup>\*a</sup> Hongjie Luo,<sup>c</sup> Litao Kang,<sup>a</sup> Zhang Chen,<sup>ab</sup> Jing Du,<sup>ab</sup> Minoru Kanehira,<sup>a</sup> Yuzhi Zhang<sup>a</sup> and Zhong Lin Wang<sup>\*d</sup>

Received 7th July 2011, Accepted 29th July 2011

DOI: 10.1039/c1ee02092g

Vanadium dioxide is a key material for thermochromic smart windows that can respond to environmental temperatures to modulate near infrared irradiation from a transparent state at low-temperature to an opaque state at high-temperature while maintaining the visible transmittance. This paper reports a novel VO<sub>2</sub>/FTO/glass multi-layered structure, which shows promising optical properties for application to energy-efficient smart windows. VO<sub>2</sub> thin films are deposited on F-doped SnO<sub>2</sub> (FTO) glasses by annealing a precursor film that is obtained *via* a solution-based process. The rutile-structured FTO substrate enhances the crystallinity of the VO<sub>2</sub> films and lowers the synthesis temperature to ~390 °C. The VO<sub>2</sub>/FTO/substrate double-layered films show both improved low-emissivity performance and distinct thermochromic properties. For a 65 nm thick VO<sub>2</sub>/FTO substrate double-layered film, low emissivities of 0.19 and 0.27 before and after the metal-insulator phase transition (MIPT) are obtained, while a solar transmittance modulation efficiency ( $\eta$ , in the wavelength range of 280–2600 nm) of 4.9% is achieved. A TiO<sub>2</sub> anti-reflective coating (ARC) is incorporated to form a three-layered TiO<sub>2</sub>/VO<sub>2</sub>/FTO/substrate structure to boost the integrated visible transmittance ( $T_{\text{vis}}$ ) while maintaining the low-emissivity performance. A 29.4% improvement for  $T_{\text{vis}}$  from 34.0% to 44.0% at room temperature is achieved for a 55 nm thick VO<sub>2</sub> film coated with a TiO<sub>2</sub> layer while emissivities of 0.13 and 0.24 before and after MIPT are maintained. Moreover,  $\eta$  is also increased significantly, from 4.3% for the VO<sub>2</sub>/FTO/substrate structure to 8.8% for the TiO<sub>2</sub>/VO<sub>2</sub>/FTO/substrate structure. Our results demonstrate a new approach of combining both thermochromism and low-emissivity performance for applications such as VO<sub>2</sub>-based energy-saving windows.

<sup>a</sup>State Key Laboratory of High Performance Ceramics and Superfine Microstructure, Shanghai Institute of Ceramics Chinese Academy of Sciences, Shanghai, 200050, China. E-mail: yfgao@mail.sic.ac.cn

<sup>b</sup>Graduate University of Chinese Academy of Sciences, 19 Yuquanlu, Beijing, 100049, China

<sup>c</sup>Industrial Ceramics Research Center, Shanghai Institute of Ceramics Chinese Academy of Sciences, Shanghai, 200050, China

<sup>d</sup>School of Materials Science and Engineering, Georgia Institute of Technology, 771 Ferst Dr N.W., Atlanta, GA, 30332, USA. E-mail: zhong.wang@mse.gatech.edu

### Broader context

Vanadium dioxide (VO<sub>2</sub>) is a well-known compound that undergoes a sharp, first order, reversible, thermally-induced, near-room temperature metal-to-insulator (MIT) transition, which is accompanied by a structural transformation from an insulating, low temperature monoclinic form VO<sub>2</sub> (M) to a high temperature rutile form VO<sub>2</sub> (R) and a dramatic change in the optical properties in the near-infrared region. The MIT near room temperature makes VO<sub>2</sub> a very promising candidate for potential applications as an energy-efficient thermochromic smart window for solar heat control. But the performance of a single layer VO<sub>2</sub> on glass is still insufficient for practical applications. Combination of this material with others that can add new functions and/or enhance the performance of VO<sub>2</sub> is an important strategy. This paper reports a novel VO<sub>2</sub>/FTO/glass multi-layered structure, which shows promising optical properties for application to energy-efficient smart windows. The rutile-structured FTO substrate enhances the crystallinity of the VO<sub>2</sub> films and lowers the synthesis temperature to ~390 °C. The VO<sub>2</sub>/FTO/substrate double-layered films show both improved low-emissivity performance and distinct thermochromic properties. A TiO<sub>2</sub> anti-reflective coating (ARC) is incorporated to form a three-layered TiO<sub>2</sub>/VO<sub>2</sub>/FTO/substrate structure to boost the integrated visible transmittance ( $T_{\text{vis}}$ ) while maintaining the low-emissivity performance.

## 1. Introduction

Buildings and maintaining man-made structures consume 30–40% of the primary energy in today's world, mainly for heating, cooling, ventilation, and lighting.<sup>1</sup> Air conditioners, in particular, are responsible for a large proportion of the energy usage. An effective control of the energy exchange between the interior and exterior of buildings through windowpanes is a key area in energy saving.<sup>1,2</sup> Thin-film coatings on building glazing to limit the amount of solar radiation entering and/or black-body radiation leaving a building is an effective strategy.<sup>1–3</sup>

In cold days, windows with high solar transmittance and low thermal emittance are needed, to admit sunlight entering and meanwhile prevent heat from escaping to keep warmth inside the house. During hot days, materials that are transparent to visible radiation but reflective to infrared (IR) radiation, such as thin metallic or transparent conductive oxides (TCOs), can be used to ensure that the inside of the building remains cool.<sup>3,4</sup> This type of smart window is made of "chromogenic" materials, which have altering optical properties in response to external stimuli.<sup>2</sup> Vanadium dioxide (VO<sub>2</sub>) is a typical example, which undergoes a reversible structural phase transition at a critical temperature ( $T_c$ ) of 68 °C.<sup>5,6</sup> At temperatures below  $T_c$ , it is in the semiconductive state with a monoclinic structure (M phase, space group  $P2_1/c$ ) that permits IR transmission. At temperatures above  $T_c$ , it is in the metallic state with a rutile lattice (R phase, space group  $P4_2/mmm$ ) that causes the material to be highly reflective or opaque in the IR region. Besides, during the phase transition, ultraviolet light is filtered off, but the transmission of visible light is almost unaffected.

Moreover, the critical temperature required for the phase transition of VO<sub>2</sub> can be adjusted to near room temperature by the introduction of dopants<sup>7,8</sup> or by reducing crystal sizes (nano-size effect).<sup>9</sup> The visible transmittance can be improved with antireflective coatings,<sup>10,11</sup> or the formation of composite films.<sup>12,13</sup> The color of the film (yellowish brown) can also be modified by incorporating metal nanoparticles.<sup>14</sup> These characteristics collectively place VO<sub>2</sub>-based materials among the most suitable alternatives for energy-saving windows.

Recent developments in our laboratory have demonstrated that solution-based processing can be used to prepare high-performance VO<sub>2</sub> films with improved visible transmittances (e.g., 62.2–83.0% at a wavelength of 650 nm for VO<sub>2</sub> films with varied film thicknesses<sup>15,16</sup>) and large near-infrared (NIR) light switching efficiencies at a wavelength of 2000 nm (e.g., 41.5% for 50 nm,<sup>15</sup> or 41.5–56.4% for VO<sub>2</sub> films with varied film thicknesses<sup>16</sup>). However, in the thermal radiation range for objects at room temperature, 3–50 μm,<sup>4</sup> the emissivities for VO<sub>2</sub> are too high, i.e., 0.83–0.84<sup>16</sup> and 0.85<sup>17</sup> for the M state, or 0.70–0.50<sup>16</sup> and 0.84<sup>17</sup> for the R state, respectively. A low-emissivity Pt layer on VO<sub>2</sub> films can depress the emissivity to 0.56 and 0.53 for the M and R states, respectively, but a distinct decrease of the visible transmittance is unavoidable.<sup>17</sup> Moreover, even with the additional Pt layer, the emissivities of the double-layered films were still too high.<sup>17</sup> A further decrease to less than 0.2 is required for VO<sub>2</sub> films to enhance their thermal insulation ability for effective energy-saving applications. Further, the deposition of VO<sub>2</sub> films by this method usually requires a high temperature,<sup>15–17</sup> likewise other solution based processing, e.g., 420–500 °C.<sup>16,18,19</sup> Effective strategies to lower the deposition temperature are in urgent need.

Transparent conductive oxides exhibit a high free-electron density and are attractive low-emissivity heat-shielding coatings because of their high IR reflection.<sup>20</sup> F:SnO<sub>2</sub> (F-doped SnO<sub>2</sub>, FTO) glass is a TCO material that is widely used in solar-energy-related applications because of its low price, high chemical stability, and excellent optical and electrical properties.<sup>21</sup> Relatively high visible transmittance (>80.0%) and low emissivity (~0.20) have been obtained for FTO-coated glasses.<sup>22,23</sup> Also, the optical constants of FTO in the visible region are between those for VO<sub>2</sub> and glass ( $n \approx 1.5$ ), which may be helpful to reduce the interface reflection and increase the visible transmittance of VO<sub>2</sub> films. An enhanced low-emissivity performance and excellent optical properties would be expected for a VO<sub>2</sub> film deposited onto FTO substrates. Furthermore, due to the similar crystalline structure of F:SnO<sub>2</sub> (JPCSD card no. 41-1445,  $P4_2/mmm$ ,  $a = 4.738 \text{ \AA}$ ,  $b = 3.187 \text{ \AA}$ ) and R-phase VO<sub>2</sub> (JPCSD card no. 44-0253,  $P4_2/mmm$ ,  $a = 4.554 \text{ \AA}$ ,  $b = 2.856 \text{ \AA}$ ), an enhanced crystallinity and a decreased deposition temperature of VO<sub>2</sub> are expected.

In this paper, FTO substrates were applied to the deposition of vanadium dioxide thin films by a polymer-assisted deposition (PAD) method.<sup>15</sup> The double-layered VO<sub>2</sub>/FTO/substrate films showed improved crystallinity and lowered synthesis temperatures (around 390 °C) than VO<sub>2</sub> deposited on amorphous fused-silica substrates. The emissivities for VO<sub>2</sub>/FTO double-layered films were depressed significantly while excellent thermochromic performances were maintained. Moreover, a TiO<sub>2</sub> ARC was deposited to boost both the visible transmittance and solar transmittance modulation abilities for the VO<sub>2</sub>/FTO films. Emissivities of 0.13 and 0.24 before and after MIPT were obtained, while  $\eta$  was as high as 8.8%. The excellent optical performance of the films reported here should further prompt the practical applications of VO<sub>2</sub>-based materials for energy-efficient windows.

## 2. Experimental and characterization procedures

VO<sub>2</sub> films were prepared as reported in previous studies.<sup>15</sup> Vanadium pentoxide (V<sub>2</sub>O<sub>5</sub>, analytically pure), polyvinylpyrrolidone (PVP, K90, average molecular weight: 1 300 000) and diamide hydrochloride (N<sub>2</sub>H<sub>4</sub>·HCl, analytically pure) were employed as starting materials to prepare the vanadium precursors. Commercial FTO glasses with sheet resistances of 14 Ω per square were rinsed in ethyl alcohol, HCl and NH<sub>3</sub>·H<sub>2</sub>O, in succession. The VO<sub>2</sub> precursor solutions were then spin-coated onto the FTO glasses. The annealing processes for the VO<sub>2</sub> films were carried out at different temperatures in a high-purity N<sub>2</sub> (99.999%) and N<sub>2</sub>-O<sub>2</sub> mixed gas atmosphere.

TiO<sub>2</sub> ARC layers were prepared as follows. First, TiO<sub>2</sub> sols were prepared using titanium tetraisopropoxide (TIPT), deionized water (the pH was adjusted to 1.10 by hydrochloride) and absolute ethanol at the volume ratio of 1 : 12 : 0.063, as described in ref. 24. The sols were kept in closed glass containers at 60 °C for a minimum of 48 h. TiO<sub>2</sub> precursor films were also obtained by spin-coating processes on the above VO<sub>2</sub> films. They were subsequently dried and annealed in vacuum at 500 °C for 30 min to obtain crystalline TiO<sub>2</sub> films. All of the reagents were from Sinopharm Chemical Reagent Co., Ltd. and used without further purification.

The annealing process of the precursor gel film was investigated by thermogravimetry/differential thermal analysis (TG-DTA, STA 449C, Netzsch, Selb, Germany) coupled with Balzers ThermoStar™ quadrupole mass spectrometer. The surface morphologies of the films were determined by field-emission scanning electron microscopy (SEM, JSM 6700F, JEOL, Tokyo, Japan). Transmission electron microscopy (TEM) images were also acquired (TEM, JEM2010, JEOL, Tokyo, Japan). Samples for cross-sectional TEM measurement were firstly polished to around 30  $\mu\text{m}$ , and then etched by Ar ion to suitable thicknesses. X-Ray diffraction was performed on a D/max 2550V X-ray diffractometer (Cu-K $\alpha$ ,  $\lambda = 0.15406$  nm). The transmittance and reflectance spectra were monitored on a UV-visible-NIR spectrophotometer (Hitachi U-4100, Japan) equipped with a custom-built heating unit. The MIPT temperatures of the thin films were measured by recording the transmittance spectra at 1500 nm as a function of temperature. The normal incident reflectance in the region of 2.5–25  $\mu\text{m}$  was measured using a Fourier-transform infrared spectrometer (FTIR, Equinox 55, Bruker, Germany) equipped with a thermo-regulated environmental cell. An Au standard film was used as a reference to measure the reflectance. The film thickness was determined using a Taylor–Hobson surface-profile measuring system by measuring at least four different points on the film. The optical constants of FTO were measured by a W-VASE with AutoRetarder™ ellipsometer, with incident angles varied at 55 and 60°. The structure and composition of the films were also characterized by Raman spectroscopy performed on a Raman microscope spectrometer (Raman, inVia Reflex, Renishaw, England) using a 514.5 nm laser.

For all samples, the integral visible transmittance ( $T_{\text{lum}}$ , 380–780 nm) and solar transmittance ( $T_{\text{sol}}$ , 240–2600 nm) were obtained based on the measured spectra using the following equation:

$$T_i = \int \varphi_i(\lambda) T(\lambda) d\lambda / \int \varphi_i(\lambda) d\lambda$$

where  $T(\lambda)$  denotes transmittance at wavelength  $\lambda$ ,  $i$  denotes lum or sol for calculations:  $\varphi_{\text{lum}}$  is the standard luminous efficiency function for the photopic vision, and  $\varphi_{\text{sol}}$  is the solar irradiance spectrum for air mass 1.5 (corresponding to the sun standing 37° above the horizon).<sup>25</sup>

For FTO glasses, the transmittance can be ignored when the wavelength is longer than 4.5  $\mu\text{m}$ . Hence, energy conservation in this region (4.5–25  $\mu\text{m}$ ) could be expressed as follows:

$$T(\lambda) + R(\lambda) + A(\lambda) \approx R(\lambda) + A(\lambda) \approx 1$$

where  $T$ ,  $R$  and  $A$  denote transmittance, reflectance and absorption in the region, respectively.

According to Kirchoff's law,

$$A(\lambda) = E(\lambda), \text{ or, } E(\lambda) = A(\lambda) = 1 - R(\lambda)$$

where  $E$  refers to the emittance, *i.e.*, the fraction of the black-body radiation.

The emissivity of films can be determined *via* weighting the film reflectance with the black-body emission spectrum from 4.5 to 25  $\mu\text{m}$ :

$$\varepsilon_T = \sum_{4.5}^{25} G_T(\lambda) E(\lambda) \Delta\lambda \approx 1 - \sum_{4.5}^{25} G_T(\lambda) R(\lambda) \Delta\lambda$$

where  $\varepsilon_T$  and  $G_T$  are the film emissivity and the normalized relative spectral distribution of black-body radiation at temperature  $T$  ( $T$  was chosen to be 20 °C according to CNS GB/T 1895.2-2002).

### 3. Results and discussion

#### 3.1. Preparation of VO<sub>2</sub> thin films from polymer-assisted deposition (PAD)

Felicitous choice of the functional group of polymer additives has significant effects on the deposition of high performance metal oxide films using the PAD process.<sup>26</sup> The metal polymer interaction in solution and/or the decomposition processes of polymers can significantly influence the crystal and growth of desired metal oxide.<sup>26</sup> In our previous reports, we had confirmed the benefits of PVP polymers on the formation of thermochromic VO<sub>2</sub> films. In solution, the PVP polymers control the viscosity and bind the VO<sub>2</sub><sup>+</sup> ions with carbonyl groups (–C=O<sup>–</sup>), resulting in a homogeneous distribution of metal precursors and the formation of uniform metal oxide films.<sup>15</sup> While in the sequence annealing process, PVP polymer decomposed and crystallized M-phase VO<sub>2</sub> films were obtained.<sup>15</sup> However, because the temperature for the crystallization of VO<sub>2</sub> and the PVP polymer degradation were nearly overlapped, these two processes were difficult to be discriminated,<sup>15</sup> or let alone, to be feasibly controlled. In the following section, we tried to figure out the influences of annealing and achieved feasible control over the above two processes.

TG/DTA-MS measurement for the PVP-k90-vanadium gel precursor in a nitrogen atmosphere was taken to investigate the effects of annealing on the decomposition of the precursor gel film and the crystallization of VO<sub>2</sub>. As shown in Fig. 1, there were three main endothermic peaks centered at 188.3 °C, 358.2 °C and 724.4 °C. The former two can be attributed to the evaporation of absorbed water and degradation of PVP polymers as indicated by CO<sub>2</sub><sup>+</sup> ( $m/z = 44$ ) and H<sub>2</sub>O<sup>+</sup> ( $m/z = 18$ ) signals in the mass spectra at the corresponding temperatures. The higher values of these two temperatures than our former results from PVP k30 (154.3 °C and 341.1 °C)<sup>15</sup> are due to the difference in molecular weight (1 300 000 for k90 and 58 000 for k30, respectively). The broad endothermic peak centered at 724.4 °C was attributed to the reduction of vanadium oxides by carbon that was decomposed from the PVP polymer. In fact, an amount of residual carbon was found after annealing of the

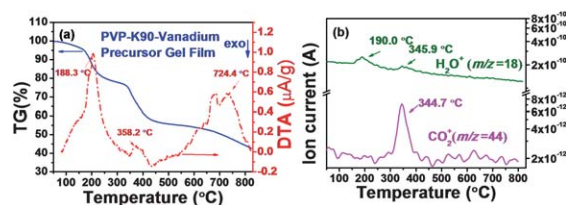
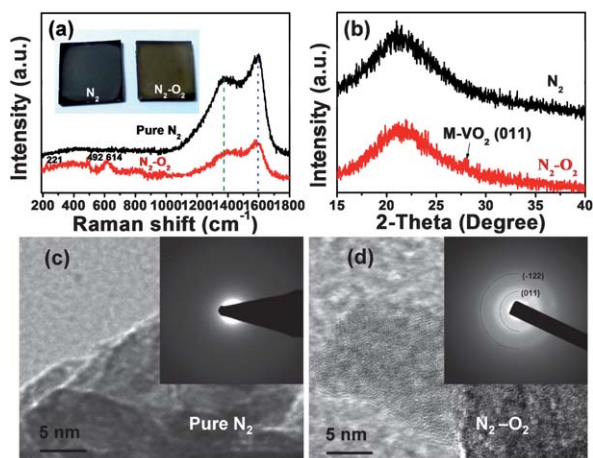


Fig. 1 TG/DAT (a) and mass spectra (MS) (b) for PVP-k90-vanadium precursor gel film annealed in a nitrogen atmosphere. The MS were taken in a carrying gas of N<sub>2</sub>.

PVP-k90-vanadium precursor gel film at above 420 °C in a high-purity nitrogen atmosphere (purity: 99.999%). As shown in Fig. 2a, the two significant shifts between 1200 and 1600 cm<sup>-1</sup> in Raman spectra for film annealed in purity N<sub>2</sub> can be assigned to disordered or graphitic carbon. Further increasing the annealing temperature resulted in the diminishing of Raman shift for carbon, and crystallized V<sub>3</sub>O<sub>5</sub> or V<sub>2</sub>O<sub>3</sub> can be found at 620 °C and 720 °C, respectively, which further confirmed that the reduction reactions occurred at the cost of carbon. No signals for gas phases in MS spectra were recorded, probably due to the coincidence of the signals for the carrying gas of N<sub>2</sub><sup>+</sup> (*m/z* = 28) with possible resultant CO<sup>+</sup> (*m/z* = 28) in the above reduction process.

The carbon residues in the films were resulted from the incomplete degradation of the PVP polymer in the N<sub>2</sub> atmosphere. Further, a carbon film could even be obtained from the PVP-only precursor in air atmosphere.<sup>27</sup> The production of carbon resulted in a significant reduction effect on the resulting films. In fact, no crystal VO<sub>2</sub> phase (M or R) was detected for precursor gel films annealed at 420 °C in a high-purity nitrogen atmosphere (99.999%), as seen in the Raman spectra (Fig. 2a), XRD (Fig. 2b) and HRTEM (Fig. 2c). To consume the carbon residues, a certain amount of oxygen was introduced by using N<sub>2</sub>-O<sub>2</sub> mixture gas (with O<sub>2</sub> of 0.1% in volume ratio), and the crystallization to VO<sub>2</sub> films occurred. Raman spectra in Fig. 2a (red line) showed distinguishable peaks centered at 221, 492, 614 cm<sup>-1</sup> for M-phase VO<sub>2</sub>,<sup>28,29</sup> although Raman modes for carbon were also observed. The weakened and broadened signals for carbon confirmed the decrease of carbon residues in the films after the introduction of oxygen. The XRD measurement also showed diffraction peaks corresponding to the M-phase VO<sub>2</sub> (JCPDS card no. 43-1051, *P*<sub>2</sub>*1*/*c*, *a* = 0.575 nm, *b* = 0.454 nm, *c* = 0.538 nm, and β = 122.64°). This result was in agreement with the finding by HRTEM (Fig. 2d) further, where the electron diffraction patterns have confirmed the formation of M-phase VO<sub>2</sub>, although the crystallinity was weak. In addition, a significant change of visual film colors from dark blue to yellowish



**Fig. 2** Room-temperature Raman spectra (a), XRD (b) and TEM (c and d) results for PVP-stabilized vanadium precursor films after annealing at 450 °C for 1 h, in a high-purity N<sub>2</sub> and N<sub>2</sub>-O<sub>2</sub> mixture atmosphere. Insets in (a) are photographs of the two films. Insets in (c) and (d) are the electron diffraction patterns of the corresponding films.

brown (typical color for M/R phase VO<sub>2</sub>) was observed. These results indicated that the annealing of the PVP-vanadium precursor gel film in N<sub>2</sub> followed an unexpectedly complicated route. The existence of oxygen and its amount can control the PVP decomposition, and therefore the VO<sub>2</sub> crystallization during annealing, which was quite encouraging for synthesizing VO<sub>2</sub> from the PAD process. Hereafter, VO<sub>2</sub> films were obtained by annealing the gel films in N<sub>2</sub> with a trace amount of oxygen (0.1% in volume). Pure VO<sub>2</sub> films with excellent optical performances were obtained.

### 3.2. Deposition of VO<sub>2</sub>/FTO/substrate double-layered films

The FTO layer had a great influence on the crystallinity of the VO<sub>2</sub> films. In a N<sub>2</sub>-O<sub>2</sub> mixture gas atmosphere (with O<sub>2</sub> of 0.1% in volume ratio), a lower synthesizing temperature of 390 °C for vanadium dioxide films could be obtained (see XRD results in Fig. 3), which is a significant decrease than that for films deposited on a fused-silica substrate (above 420 °C as mentioned previously). These results indicate that the rutile FTO substrate induced the growth of VO<sub>2</sub>, which may be because FTO and VO<sub>2</sub> possess a same crystalline structure and similar lattice indexes. The growth of VO<sub>2</sub> on the FTO surface has a lower nucleation barrier. For films annealed at 510 °C, in addition to the diffraction peaks from FTO, diffraction peaks corresponding to the M-phase VO<sub>2</sub> were observed, and the XRD patterns showed that the VO<sub>2</sub> exhibited a preferred orientation of (011). The XRD results also showed a narrower full-width at half-maximum (FWHM) of the main peak of VO<sub>2</sub> film deposited on FTO than that deposited on a fused-silica substrate at the same temperature (0.24° vs. 0.34°, see inset of Fig. 3). These results indicate an increased crystallinity of VO<sub>2</sub> films on FTO-coated glass. Similar results have been observed for VO<sub>2</sub> films deposited on rutile TiO<sub>2</sub>-buffered substrates.<sup>30,31</sup> No diffraction patterns corresponding to other vanadium oxides (*e.g.*, V<sub>6</sub>O<sub>13</sub>, V<sub>2</sub>O<sub>5</sub>) were detected. The increased crystallinity and lowered synthesis temperature should further promote the practical applications for VO<sub>2</sub>-based energy-saving windows.

Room-temperature Raman spectra were also taken to confirm the structure and composition of the as-obtained films, and the results are shown in Fig. 4. Raman modes corresponding to the

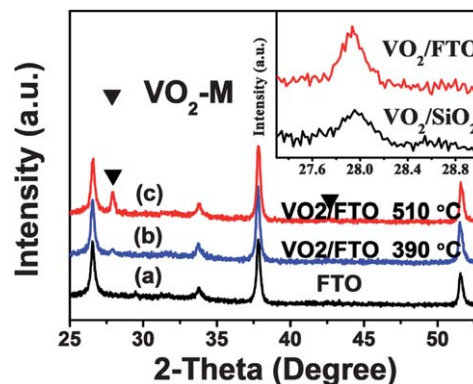


**Fig. 3** XRD results for the FTO substrate (a) and the VO<sub>2</sub>/FTO substrate films after annealing at 390 °C (b) and 510 °C (c) in a N<sub>2</sub>-O<sub>2</sub> mixture atmosphere. The inset shows the enlarged XRD pattern for VO<sub>2</sub> films deposited on FTO and fused-silica substrates.

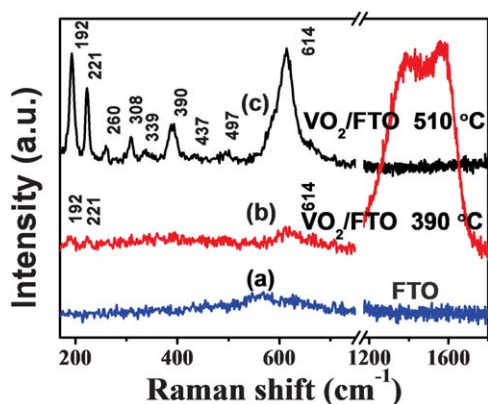


**Fig. 4** Room-temperature Raman spectra for the FTO substrate (a) and the VO<sub>2</sub>/FTO/substrate films obtained by annealing at 390 °C (b) and 510 °C (c), respectively.

M-phase VO<sub>2</sub> were found for films after annealing,<sup>28,29</sup> with distinguishable peaks centered at 192, 221, and 614 cm<sup>-1</sup> at 390 °C, and at 192, 221, 260, 308, 338, 390, 437, 497, and 614 cm<sup>-1</sup> at 510 °C. No Raman modes corresponding to other vanadium oxides (*e.g.*, V<sub>6</sub>O<sub>13</sub>, V<sub>2</sub>O<sub>5</sub>, V<sub>2</sub>O<sub>3</sub>) were detected within the accuracy of the measurements ( $\pm 0.2$  cm<sup>-1</sup>). These results indicate the formation of a M-phase VO<sub>2</sub> film at 390 °C, in accordance with the XRD results. However, the two significant Raman shifts for carbon (between 1200 and 1600 cm<sup>-1</sup>) were also observed for this VO<sub>2</sub> film. These shifts disappeared for the film after annealing at 510 °C. Therefore, to obtain pure VO<sub>2</sub> films and thus avoid the influences of other phases (*e.g.*, carbon), all films were synthesized at 510 °C for following experiments.

The SEM morphologies for the VO<sub>2</sub> films deposited on FTO substrates at 510 °C are shown in Fig. 5. The FTO layer was composed of a pyramid-like top surface with large surface roughness. After deposition of the VO<sub>2</sub> films, the valleys among these pyramids were filled by VO<sub>2</sub> particles with uneven sizes. Cross-sectional SEM morphologies (Fig. 5d) showed that these large VO<sub>2</sub> particles (marked with red arrows in Fig. 5c) were in fact grown on the top surfaces of the FTO columns. Because of the low solid-solubility of SnO<sub>2</sub> and vanadium oxides,<sup>32,33</sup> no significant interface diffusion between FTO and VO<sub>2</sub> was observed by element line scan from STEM. Moreover, a HRTEM image of the VO<sub>2</sub> and FTO interfaces in Fig. 5d confirmed the epitaxial growth of VO<sub>2</sub> on FTO crystal lattices. The growth of VO<sub>2</sub> particles can be promoted on rutile-structured FTO particles, which cause the uneven growth of the VO<sub>2</sub> particles. Indeed, rutile VO<sub>x</sub> ( $x \approx 2$ ) were reported to be stabilized and had promotable epitaxial growth on SnO<sub>2</sub> (110) surfaces.<sup>34</sup> These results confirmed the benefits of FTO on the crystallization and growth of VO<sub>2</sub> films.

### 3.3. Characterization of thermochromism and emissivity properties

The thickness-dependence of the optical properties of VO<sub>2</sub>/FTO double-layered films is shown in Fig. 6. Unlike the typical spectra for VO<sub>2</sub> films deposited on fused silica (see ref. 16 and 30), the transmittance in the NIR region for the M and R states was greatly depressed by the strong absorption and reflection of FTO

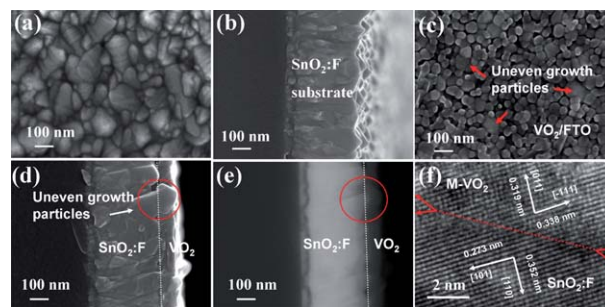


**Fig. 5** SEM and HRTEM photographs for the FTO substrate and VO<sub>2</sub>/FTO/substrate double-layered films. (a and b) and (c and d) are the surface and cross-sectional morphologies for the FTO substrate and the VO<sub>2</sub>/FTO/substrate double-layered film. (e) is the backscattered electron image for the VO<sub>2</sub>/FTO/substrate double-layered film. The arrows and circle in (c and d) show the uneven growth of VO<sub>2</sub> particles. (f) is the HRTEM image for the interface of FTO and VO<sub>2</sub>.

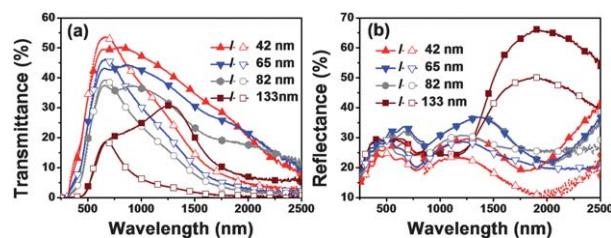


**Fig. 6** Transmittance (a) and reflectance (b) spectra for the VO<sub>2</sub>/FTO/substrate double-layered films with different thicknesses. Lines with solid and open symbols are the spectra measured at 20 °C and 90 °C, respectively.

in this region. Moreover, as evident in Fig. 6, the visible transmittance ( $T_{\text{vis}}$ ) for these films decreased distinctly with increasing film thickness, which was mainly attributed to the absorption of VO<sub>2</sub> films in the visible region (380–780 nm). The decreased value of  $T_{\text{vis}}$  resulted from the difference in the visible transmittances of the substrates (82.4% vs. larger than 92.8% for FTO and fused-silica substrates<sup>15,16</sup>). However, the visible transmittance was still encouraging for VO<sub>2</sub>/FTO double-layered films deposited by our methods. For a 42 nm thick VO<sub>2</sub> film deposited on FTO glass, the  $T_{\text{vis}}$  reached 39.6% and 35.9% for M and R states, which is similar in transparency with pure VO<sub>2</sub> films deposited on transparent Al<sub>2</sub>O<sub>3</sub> substrates by vapor-phase methods (34.2% and 37.1% for S and M states for 40 nm thick films<sup>35,36</sup>). Furthermore, when considering the low-emissivity

**Table 1** Summary of optical properties of the VO<sub>2</sub>/FTO double-layered films with different thicknesses that were deposited on FTO glasses at 510 °C for 3 h. Solar transmittance modulation (STM) was calculated from the transmittance spectra in Fig. 3

Thickness of VO <sub>2</sub> on FTO/nm	$T_{\text{vis-20 °C}}$ (%)	$T_{\text{vis-90 °C}}$ (%)	STM (%)
42	39.6	35.9	3.5
65	34.0	28.6	4.9
82	28.0	23.9	4.8
133	14.9	8.2	7.1

performance discussed later, the optical properties of the VO<sub>2</sub>/FTO double-layered films were quite good.

Moreover, the solar transmittance modulation ability was reduced because of the depressed NIR transmittance of the FTO substrates (only 62.6% of the total solar energy in the NIR region was transmitted throughout the FTO substrate). A summary of the optical properties for these films is given in Table 1. As seen in Table 1, there is a tradeoff between the solar transmittance modulation ability and the visible transmittance; increasing film thickness results in higher solar transmittance modulation ability but lower visible transmittance. A tactful layer design would be required to synchronously boost the visible transmittance and solar transmittance modulation, which will be discussed in the subsequent section.

The emissivity of VO<sub>2</sub>/FTO double-layered films was studied by measuring the normal incidence reflectance in the wavelength range of 2.5–25 μm at both room temperature (20 °C) and 90 °C (Fig. 7). A reflectance spectrum for a 68 nm thick VO<sub>2</sub> film on a fused-silica substrate was also collected for comparison. The reflectance peaks at approximately 8–10 μm and 20–25 μm were signals from the fused-silica substrate.<sup>16</sup> For the VO<sub>2</sub>/FTO double-layered films, the IR reflectance spectra (Fig. 7) for both the M and R phases were greatly enhanced, resulting in lower emissivities. The thickness dependence of the emissivity for these films is shown in Fig. 8. An abnormal phenomenon is observed in

both Fig. 7 and 8, where the semiconductor state showed higher reflectance or lower emissivity than the metallic state.

The low emissivity of FTO substrates and the changeable IR optical properties of VO<sub>2</sub> films across the phase transition should create special emissivity evolutions. As discussed previously, solution-deposited VO<sub>2</sub> films exhibited quite high thermal emissivities, even in the metallic state.<sup>16</sup> A strong absorptive feature, especially for the R-phase VO<sub>2</sub>, was confirmed by the increasing trend of emissivity or absorption for VO<sub>2</sub>/FTO double-layered films by increasing the VO<sub>2</sub> thicknesses (Fig. 8). In fact, the absorption coefficient at 10 μm for VO<sub>2</sub> can be increased from  $\sim 6.3 \times 10^{-5}$  to  $\sim 1.0 \times 10^{-2}$  before and after the MIPT, as calculated in the ref. 37. Moreover, the absorption from the surface and interface because of the porous structure of our VO<sub>2</sub> films may also play an important role. For VO<sub>2</sub>/FTO films in the M state, the emissivities are similar to the FTO substrate (0.12 at 20 °C) because of the high IR transparency of VO<sub>2</sub>. However, when the film was transformed to the R state with strong absorption, the emissivity increased above that for the FTO substrate (0.13 at 90 °C). Similar results with decreased IR reflectance after the MIPT have been reported previously, although the VO<sub>2</sub> films were deposited on a low-emissivity Al substrate.<sup>38</sup> Moreover, the increased absorption in the IR region for the R state can cause a more significant increase in the emissivity than the M state by increasing the thickness of VO<sub>2</sub> films, as observed in Fig. 8.

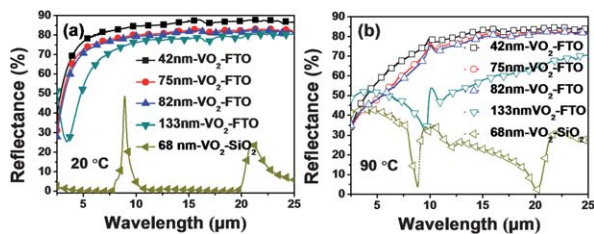


**Fig. 7** Normal incidence reflectance spectra measured at 20 °C (a) and 90 °C (b) for the VO<sub>2</sub>/FTO/substrate double-layered films with different thicknesses. The results for a 68 nm thick VO<sub>2</sub> film deposited on a fused-silica substrate are given for comparison.

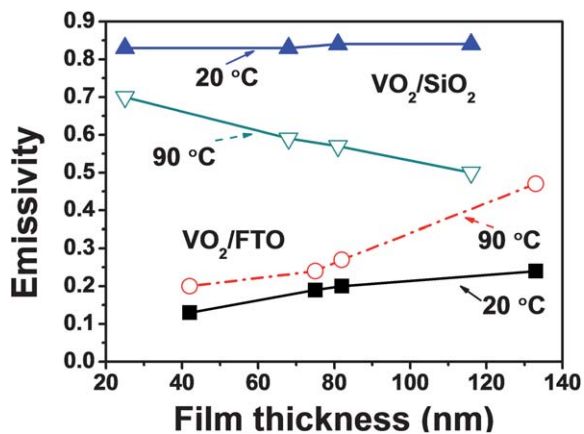


**Fig. 8** Thickness-dependence of emissivity for the VO<sub>2</sub>/FTO/substrate films. The emissivity for VO<sub>2</sub> on fused-silica substrates was adopted for comparison.<sup>16</sup> Lines with solid and open circles are the emissivities measured at 20 °C and 90 °C, respectively.

### 3.4. TiO<sub>2</sub> ARC strategy

According to Fig. 6, the VO<sub>2</sub>/FTO double-layered films showed relatively low visible transparency compared to our previous reports, and strong reflection in the visible region was observed. To suppress these reflections, TiO<sub>2</sub> ARCs were applied. As discussed by others,<sup>39,40</sup> TiO<sub>2</sub> could serve as an effective ARC to enhance the visible transmittance of VO<sub>2</sub> films because of its suitable optical constants in the visible region ( $2.2 \leq n \leq 2.5$  at 550 nm for TiO<sub>2</sub> with optimized  $n$  in the range of 2.0 to 2.4<sup>10</sup>). Moreover, TiO<sub>2</sub> is transparent in a wide-infrared region, which would cause no significant absorptance of IR light, as observed for the R-phase VO<sub>2</sub>. In fact, TiO<sub>2</sub> is among the most widely used materials for thermal-insulating or heat-mirroring strategies. For practical applications to smart windows, the TiO<sub>2</sub> layer can have multi-functions including photocatalytic and self-cleaning properties. Besides, a significant improvement of oxidation durability is also achieved by the addition of the TiO<sub>2</sub> capping layers. Based on these considerations, a thin layer of TiO<sub>2</sub> ARCs were deposited on the VO<sub>2</sub>/FTO films.

To obtain high anti-reflection abilities, the thickness of TiO<sub>2</sub> ARC layer was optimized based on our former investigation.<sup>41</sup> The refractive index (RI) of VO<sub>2</sub> is different for the semi-conductive state and the metallic state; the metallic state has a lower RI. We have confirmed that for a half-quarter-waved structure, when the thickness of the TiO<sub>2</sub> ARC layer was in the optimized region for VO<sub>2</sub> at 20 °C, the reflection minima at 90 °C appear at a shorter wavelength.<sup>41</sup> In this case, the transmittance difference at 20 °C and 90 °C can be enlarged, and both visible transmittance and solar transmittance modulation ability can be improved.<sup>41</sup> A TiO<sub>2</sub> ARC layer should work well for the VO<sub>2</sub>/FTO glass multilayered structure.

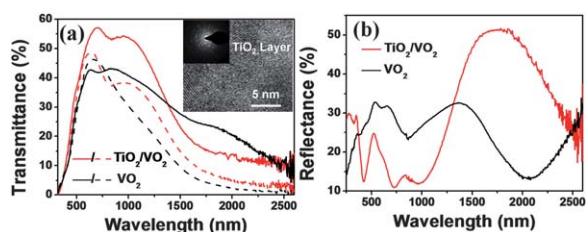


**Fig. 9** Transmittance (a) and reflectance (b) spectra for the VO<sub>2</sub>/FTO/substrate double-layered films without and with a TiO<sub>2</sub> layer. The solid and dotted lines are the spectra measured at 20 °C and 90 °C, respectively. The inset in (a) shows the high-resolution TEM image for polycrystalline TiO<sub>2</sub> layers.

Fig. 9 shows the transmittance and reflectance spectra of a 55 nm VO<sub>2</sub> film with and without TiO<sub>2</sub> (60 nm thick). As evident from the reflectance spectra (Fig. 9b), the reflectance was significantly reduced in the visible region with the TiO<sub>2</sub> coating, *i.e.*, from 32.6% to 23.1% at 550 nm at room temperature; the integrated visible transmittance was improved from 34.0% and 35.1% at 20 °C to 44.0% and 38.2% at 90 °C, respectively. Moreover, a great increase in solar transmittance modulation ability (in the range of 240–2600 nm) was also obtained: from 4.35% to 8.81% without and with the ARC. This was due to the large reduction of transmittance at short-wave NIR wavelengths, which carry more solar energy than longer-wavelength radiation, based on the solar irradiance spectrum for air mass 1.5. The addition of a TiO<sub>2</sub> ARC could work as an efficient functional layer to boost both visible transmittance and solar modulation ability. This result was quite encouraging, especially for the application of VO<sub>2</sub>/FTO double-layered films in energy-saving windows.

In addition, the deposition of TiO<sub>2</sub> ARCs obviously influences the phase-transition properties. Hysteresis loops during the heating and cooling of samples with and without a TiO<sub>2</sub> layer are shown in Fig. 10. The original VO<sub>2</sub> film shows a broad hysteresis loop width of 25.7 °C, in agreement with the typical characteristics of polycrystalline VO<sub>2</sub> films. A step appeared in the cooling curve, which is probably related to the distinct size distributions

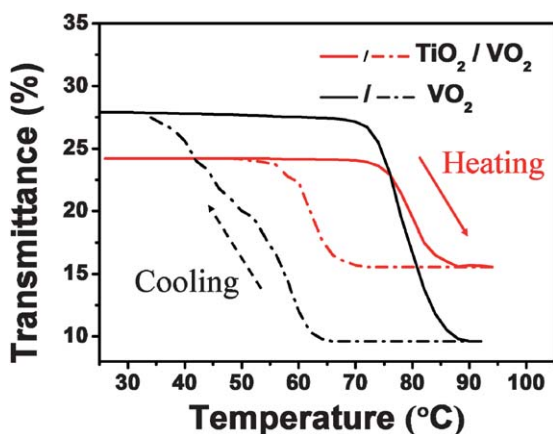


**Fig. 10** Hysteresis loops for the VO<sub>2</sub>/FTO/substrate double-layered films and the TiO<sub>2</sub>/VO<sub>2</sub>/FTO/substrate triple-layered films obtained by measuring the transmittances at 1500 nm with heating (solid lines) and cooling (dash-dotted lines).

of normal-sized particles and particles with uneven growth.<sup>42,43</sup> However, for the TiO<sub>2</sub>/VO<sub>2</sub>/FTO/substrate film, the hysteresis loop width was narrowed to 17.4 °C and the MIPT temperature was increased from 65 to 71.0 °C. The narrowed hysteresis width and increased MIPT temperature originated from the Ti<sup>4+</sup> diffusion and doping of Ti<sup>4+</sup> into VO<sub>2</sub> lattices during the heat treatment at 500 °C,<sup>30</sup> which was confirmed by STEM characterization.

The IR reflection spectra for VO<sub>2</sub> films deposited with and without TiO<sub>2</sub> films are shown in Fig. 11. Both films showed similar reflectance values at wavelengths greater than 4.5 μm at room temperature. However, an increase in the reflectance, especially at wavelengths greater than 6.3 μm, for TiO<sub>2</sub>-coated VO<sub>2</sub> films was observed after the MIPT. The emissivities at S and M states were 0.13 and 0.29 for the VO<sub>2</sub>/FTO films, and 0.13 and 0.24 for the TiO<sub>2</sub>/VO<sub>2</sub>/FTO films, respectively; this result indicates a decrease of the emissivity after the application of the TiO<sub>2</sub> coatings. Moreover, an adverse increase in emissivity at the R state (observed in Fig. 8) was also improved to some extent. As discussed above, VO<sub>2</sub> films deposited on FTO substrates exhibited a transparent character for IR light in the semi-conductive state, while a highly absorptive character in the metallic states. However, after the deposition of the TiO<sub>2</sub> layer, a certain amount of Ti<sup>4+</sup> diffused and doped into the VO<sub>2</sub> crystals. The Ti<sup>4+</sup> (3d<sup>0</sup>) provides one less 3d electron than VO<sub>2</sub> (3d<sup>1</sup>) to the conduction band, thereby causing a decrease in the carrier concentration that was absorptive for IR light.<sup>6</sup> Systematic studies of the influence of Ti doping on the emissivity are being carried out. However, the benefits of TiO<sub>2</sub> coatings on the thermochromic properties and the emissivity performance are confirmed, which are interesting for the practical applications of VO<sub>2</sub>-based smart windows.

VO<sub>2</sub> films can intelligently modulate solar heat due to the temperature-responsive MIPT, but the performance of a single layer VO<sub>2</sub> on glass is still insufficient for practical applications. Combination of this material with others that can add new functions and/or enhance the performance of VO<sub>2</sub> is an important strategy. For this purpose, an infrared reflectance layer or a low-emissivity layer is favorable. This study shows that a visible

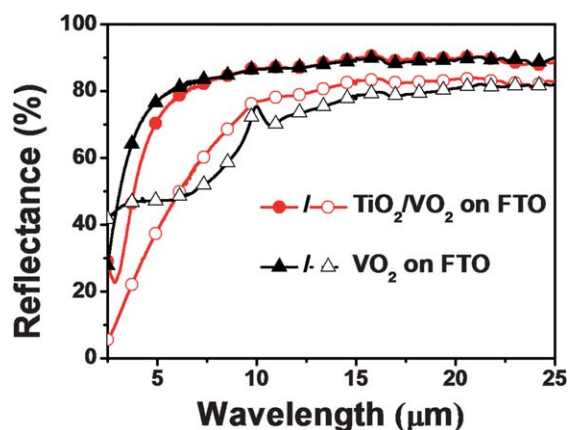


**Fig. 11** Normal incident reflectance spectra for the VO<sub>2</sub>/FTO/substrate films with (red circle lines) and without TiO<sub>2</sub> layers (black up-triangle lines). The lines with solid and open symbols are spectra measured at 20 °C and 90 °C, respectively.

transparent F:SnO<sub>2</sub> layer with an adequate thickness can add high infrared reflectance or low-emissivity to VO<sub>2</sub>-based materials, and the FTO layer can also induce VO<sub>2</sub> crystallization because both have the similar crystal structure. For a multi-layered structure, the thickness optimization is an important issue; the determination should consider the function of a specific layer and the synergetic performance of a multi-layer structure, and can be achieved experimentally or by optical simulation. The ARC layer can improve both visible transmittance and solar modulation ability, and other functions such as photocatalytic, self-cleaning or anti-oxidization properties. The structure in this paper provided a novel prototype of VO<sub>2</sub>-based energy-saving windows.

#### 4. Conclusions

In this paper, thermochromic vanadium dioxide thin films were deposited on transparent conducting FTO substrates using a lower-temperature solution process. The VO<sub>2</sub> films on FTO glass showed improved crystallinity and a lowered synthesis temperature compared to films deposited on amorphous fused-silica substrates. VO<sub>2</sub> films deposited on FTO substrates showed significant thermochromic properties, and low emissivity could be reached for both the semiconducting and metallic states. This behavior is beneficial for energy-saving smart windows. For a 42 nm thick VO<sub>2</sub> film deposited on FTO glass, a visible transmittance of 39.6% and 35.9% was obtained for the S and M states, respectively. The emissivity for the samples was quite low (0.15 and 0.19 for S and M states), whereas a solar transmittance modulation of 3.5% was achieved. An ARC with a TiO<sub>2</sub> layer was applied to boost the optical performance of the films. For a 55 nm thick VO<sub>2</sub> film, the calculated  $T_{\text{vis}}$  values increased from 34.0% to 44.0%, whereas solar transmittance modulation was improved from 4.35% to 8.81%. Moreover, the emissivities were sustained, and an improvement of the low-emissivity performance was observed in the metallic state after the application of the TiO<sub>2</sub> coatings. The results are encouraging because they open new avenues to achieve excellent thermochromic properties coupled with low-emissivity performance.

#### Acknowledgements

This study was supported in part by the Century Program (One-Hundred-Talent Program) of the Chinese Academy of Sciences, National Key Basic Research Project (NKBRP, 2009CB939904), the National Natural Science Foundation of China (NSFC, contract no: 50772126, 51032008), Shanghai Key Basic Research Project (09DJ1400200), Shanghai Basic Research Project (08JC1420300), The key project of the Chinese Academy of Sciences (grant no. 4912009YC006) and Shanghai Talent Project of Science and Technology (Pujiang Talent Program, 09PJ1410700).

#### Notes and references

- 1 I. P. Parkin and T. D. Manning, *J. Chem. Educ.*, 2006, **83**, 393.
- 2 C. G. Granqvist, P. C. Lansåker, N. R. Mlyuka, G. A. Niklasson and E. Avendaño, *Sol. Energy Mater. Sol. Cells*, 2009, **93**, 2032.
- 3 S. S. Kanu and R. Binions, *Proc. - R. Soc. Edinburgh, Sect. A: Math*, 2010, **466**, 19.
- 4 C. G. Granqvist, *Adv. Mater.*, 2003, **15**, 1789.
- 5 F. J. Morin, *Phys. Rev. Lett.*, 1959, **3**, 34.

- 6 J. B. Goodenough, *J. Solid State Chem.*, 1971, **3**, 490.
- 7 C. H. Griffiths and H. K. Eastwood, *J. Appl. Phys.*, 1974, **45**, 2201.
- 8 S. H. Chen, H. Ma, J. Dai and X. J. Yi, *Appl. Phys. Lett.*, 2007, **90**, 101117.
- 9 L. Dai, C. X. Cao, Y. F. Gao and H. J. Luo, *Sol. Energy Mater. Sol. Cells*, 2011, **95**, 712.
- 10 G. Xu, P. Jin, M. Tazawa and K. Yoshimura, *Sol. Energy Mater. Sol. Cells*, 2004, **83**, 29.
- 11 N. R. Mlyuka, G. A. Niklasson and C. G. Granqvist, *Sol. Energy Mater. Sol. Cells*, 2009, **93**, 1685.
- 12 J. Du, Y. F. Gao, H. J. Luo, L. T. Kang, Z. T. Zhang and C. X. Cao, *Sol. Energy Mater. Sol. Cells*, 2011, **95**, 469.
- 13 U. Qureshi, T. D. Manning, C. Blackman and I. P. Parkin, *Polyhedron*, 2006, **25**, 334.
- 14 M. Saeli, C. Piccirillo, I. P. Parkin, I. Ridley and R. Binions, *Sol. Energy Mater. Sol. Cells*, 2010, **94**, 141.
- 15 L. T. Kang, Y. F. Gao and H. J. Luo, *ACS Appl. Mater. Interfaces*, 2009, **1**, 2211.
- 16 Z. T. Zhang, Y. F. Gao, Z. Chen, J. Du, C. X. Cao, L. T. Kang and H. J. Luo, *Langmuir*, 2010, **26**, 10738.
- 17 L. T. Kang, Y. F. Gao, Z. Chen, J. Du, Z. T. Zhang and H. J. Luo, *Sol. Energy Mater. Sol. Cells*, 2010, **94**, 2078.
- 18 F. Beteille and J. Livage, *J. Sol-Gel Sci. Technol.*, 1998, **13**, 915.
- 19 J. Livage, G. Guzman, F. Beteille and P. Davidson, *J. Sol-Gel Sci. Technol.*, 1997, **8**, 857.
- 20 H. L. Hartnagel, A. L. Dawar, A. K. Jain and C. Jagadish, in *Semiconducting Transparent Thin Films*, Institute of Physics Publishing, Bristol, England 1995.
- 21 T. Fukano, T. Motohiro, T. Ida and H. Hashizume, *J. Appl. Phys.*, 2005, **97**, 084314.
- 22 Y. Z. Gao, R. Yang, Y. Gao and J. Shen, *Mater. Sci. Forum*, 2010, **658**, 81.
- 23 E. L. Bourhis, in *Glass: Mechanics and Technology*, Wiley-VCH, Weinheim, 2007, chapter 4, p.42.
- 24 M. B. M. Langlet, C. Coutier, C. Jimenez, C. Morant and M. Manso, *J. Sol-Gel Sci. Technol.*, 2001, **22**, 139.
- 25 *ASTM*, Vol. G173-03, 2003.
- 26 A. K. Burrell, T. M. McCleskey and Q. X. Jia, *Chem. Commun.*, 2008, **11**, 1271.
- 27 A. B. Bourlinos, V. Georgakilas and R. Zboril, *Carbon*, 2008, **46**, 1792.
- 28 G. I. Petrov, V. V. Yakovlev and J. Squier, *Appl. Phys. Lett.*, 2002, **81**, 1023.
- 29 T. D. Manning, I. P. Parkin, M. E. Pemble, D. Sheel and D. Vernardou, *Chem. Mater.*, 2004, **16**, 744.
- 30 Z. T. Zhang, Y. F. Gao, L. T. Kang, J. Du and H. J. Luo, *J. Phys. Chem. C*, 2011, **114**, 22214.
- 31 G. Fu, A. Polity, N. Volbers and B. K. Meyer, *Thin Solid Films*, 2006, **515**, 2519.
- 32 S. Bordoni, F. Cavani, F. Trifirò and M. J. Gazzano, *J. Chem. Soc., Faraday Trans.*, 1994, **90**, 2981.
- 33 A. E. Taverner, C. Rayden, S. Warren, A. Gulino, P. A. Cox and R. G. Egdell, *Phys. Rev. B: Condens. Matter*, 1995, **51**, 6833.
- 34 A. Atrèi, T. Cecconi, B. Cortigiani, U. Bardi, M. Torrini and G. Roviada, *Surf. Sci.*, 2002, **513**, 149.
- 35 G. Xu, P. Jin, M. Tazawa and K. Yoshimura, *Appl. Surf. Sci.*, 2005, **244**, 449.
- 36 G. Xu, P. Jin, M. Tazawa and K. Yoshimura, *Jpn. J. Appl. Phys.*, 2004, **43**, 186.
- 37 F. Guinneton, L. Sauques, J. C. Valmalette, F. Cros and J. R. Gavarrì, *Thin Solid Films*, 2004, **446**, 287.
- 38 J. I. Kleiman, R. V. Kruzelecky, E. Haddad, B. Wong, W. E. S. Jamroz, M. Soltani, M. Chaker, D. Nikanpour and X. X. Jiang, in *Protection of Materials and Structures from the Space Environment*, Springer, Netherlands, 2006, vol. 6, p. 277.
- 39 P. Jin, G. Xu, M. Tazawa and K. Yoshimura, *Appl. Phys. A: Mater. Sci. Process.*, 2003, **77**, 455.
- 40 P. Jin, G. Xu, M. Tazawa and K. Yoshimura, *Jpn. J. Appl. Phys.*, 2002, **41**, L278.
- 41 Z. Chen, Y. F. Gao, L. T. Kang, J. Du, Z. T. Zhang, H. J. Luo, H. Y. Miao and G. Q. Tan, *Sol. Energy Mater. Sol. Cells*, 2011, **95**, 2677–2684.
- 42 L. T. Kang, Y. F. Gao, Z. T. Zhang, J. Du, C. X. Cao, Z. Chen and H. J. Luo, *J. Phys. Chem. C*, 2010, **114**, 1901.
- 43 R. Aliev and V. Klimov, *Phys. Solid State*, 2004, **46**, 532.